Velocity-Vorticity Decomposition of the Reynolds Stress Gradient in a Shear Layer

Scott C. Morris
Department of Aerospace and Mechanical Engineering
University of Notre Dame
Notre Dame, IN 46556 USA
morris.65@nd.edu

John F. Foss, Aren Hellum
Department of Mechanical Engineering
Michigan State University
East Lansing, MI 48824 USA
foss@egr.msu.edu

ABSTRACT

Time series measurements of velocity and vorticity using a four sensor hot-wire technique have been acquired in a large scale single stream shear layer. The Reynolds stress gradient which appears in the time averaged momentum equation can be written in terms of velocity-vorticity products. The experimental data allows for the evaluation of these quantities, and the spectral content of the time series provides insight into the scales of motion which lead to the time averaged values.

The power spectral density function for the vorticity time series (ω_z, ω_y) show substantial values at a wide range of wave numbers. The velocity-vorticity products also indicates a wide distribution in wave number space. This indicates the existence of anisotropic motions which contribute to the Reynolds shear stress gradient at wave numbers at both very high and very low wave numbers.

INTRODUCTION

The Reynolds averaged Navier-Stokes equations can be written as:

$$\bar{u}_j \frac{\partial \bar{u}_i}{\partial x_j} = \frac{1}{\rho}\frac{\partial}{\partial x_j}(-\bar{P}\delta_{ij} + 2\mu\bar{S}_{ij} - \rho\overline{u'_i u'_j}) \qquad (1)$$

where $\bar{S}_{ij}$ represents the time averaged rate of strain tensor. The modeling of the Reynolds stress $\overline{u'_i u'_j}$ is the subject of considerable research; see, e.g., Pope 2000 for a review. The physical mechanisms which lead to the Reynolds stresses are still a topic of research, since no universal model has been found that relates these terms to the mean flow variables. Empirical and heuristic models often encounter problems when varied physical mechanisms are responsible for the generation of Reynolds stresses within a given domain.

The single stream shear layer provides an interesting boundary value problem in which to study the Reynolds stresses. The only non-zero component of the Reynolds shear stress tensor is $\overline{u'v'}$. This term appears in the boundary layer form of the momentum equation:

$$\bar{u}\frac{\partial \bar{u}}{\partial x} + \bar{v}\frac{\partial \bar{u}}{\partial y} = -\frac{\partial \overline{u'v'}}{\partial y} \qquad (2)$$

which, for the flow field considered herein, appropriately assumes that the mean viscous stress, pressure gradients, and streamwise gradients are negligible. The present examination of the Reynolds stress gradient begins with the identity (again, ignoring streamwise gradients):

$$-\frac{\partial \overline{u'v'}}{\partial y} \approx \overline{v'\omega'}_z - \overline{w'\omega'}_y . \qquad (3)$$

Tennekes and Lumley [2] provide an interpretation of this expression in terms of a pseudo body force which results from the velocity-vorticity correlations. Equation (3) then indicates that the net shear stress gradient is a result of contributions from (or cancellations of) the two velocity-vorticity products.

The subject of this paper is the direct measurement of the time series data of the terms of equation 3. This provides a unique opportunity to observe the scales of motion (in terms of spectral content) of the *gradient* of the Reynolds stress.

DESCRIPTION OF EXPERIMENT

A large scale single stream shear layer facility located at the Turbulent Shear Flows Laboratory of Michigan State University was used for the experiments; see Figure 1. The Reynolds number of the boundary layer at separation is Re_θ=4650, based on the momentum thickness $\theta(x=0)=\theta_o$=9.6mm, and the constant free stream velocity: U_o=7.1m/s. The shear layer test section is 9.7m in length from the separation point to the tunnel exit. A low disturbance level entrainment flow is delivered

through four axial fans to maintain a zero pressure gradient test section.

Spanwise vorticity measurements have been acquired using the compact four sensor hot-wire probe developed by Foss and coworkers, see, e.g., Haw et al. (1989) and demonstrated by Wallace and Foss (1995). A schematic representation of the probe is shown in Figure 2. The two parallel wires record the magnitude of velocity with a small ($\delta y \sim 1.4$mm) spatial separation. The sensors configured as an X-array are used to recover the v component of velocity. From these three signals, a micro circulation domain is constructed with the flow direction calculated using a convected distance from the local (in time) velocity magnitude. This is shown schematically in Figure 3. The resolution of the micro circulation domain in the present experiment is approximately 7 Kolmogorov length scales.

The vorticity probe was traversed across the shear layer at the streamwise location: $x/\theta_o=675$. Time series data were acquired at 40kHz for 50 seconds. The Reynolds number of the shear layer at this location was $Re_\theta=150{,}000$ based on the local momentum thickness.

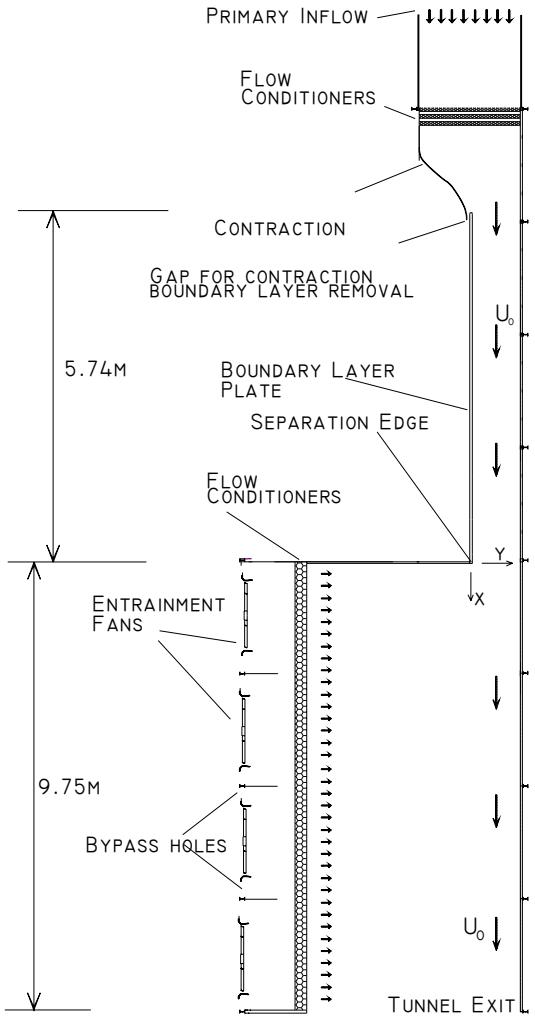

Figure 1. Schematic of the single stream shear layer facility.

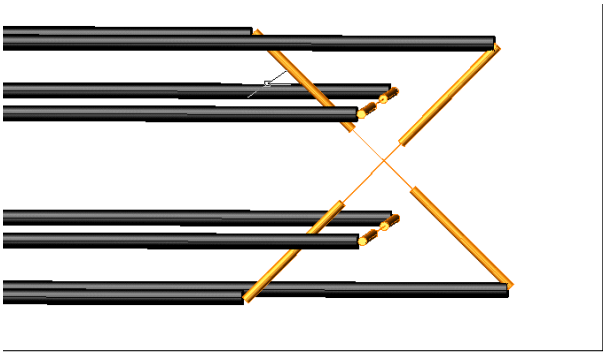

Figure 2. Schematic of the four wire vorticity probe. Note the distance between the parallel wires is typically 1.5mm.

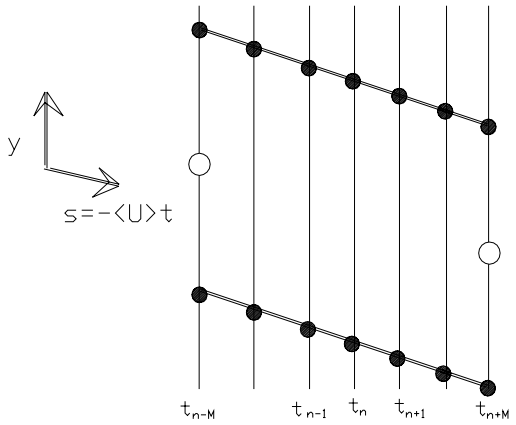

Figure 3. Diagram of the micro circulation domain used to calculate vorticity from the four wire probe.

RESULTS AND DISCUSSION

The time averaged velocity distribution: $\bar{u}(y)$, exhibits excellent self-preservation ($x/\theta(0)>100$), see Fig. 4. The mean velocity field, with the assumption of self similarity, can be used to evaluate the non-dimensional Reynolds stress: $h(y) \equiv (1/\sigma)[\overline{u'v'}/U_o^2]$ shown in Fig. 5 along with the directly measured values. The Reynods stress gradient: $h'(y) \equiv (1/\sigma)\partial[\overline{u'v'}/U_o^2]/\partial(y/\theta)$, where $\sigma=d\theta/dx$ and $\eta=(y-y_{1/2})/\theta$ is shown in Fig. 6.

The measured values obtained at $x/\theta o=675$, $\eta=0$ will be used for the present communication. Several statistics of interest at this location include, where [~] indicates standard deviation:

$$\bar{u}/U_o = 0.508\,,\ \tilde{u}/U_o = 0.157\,,\ \tilde{v}/U_o = 0.118$$

$$\tilde{w}/U_o = 0.136\,,\ \overline{u'v'}/(\tilde{u}\tilde{v}) = 0.413$$

$$\tilde{\omega}_z\lambda_u/\tilde{u} = 0.92\,,\ \tilde{\omega}_y\lambda_u/\tilde{u} = 0.58$$

where λ_u is the Taylor microscale and the vorticity scalings reflect the dissipative scales of the flow field.

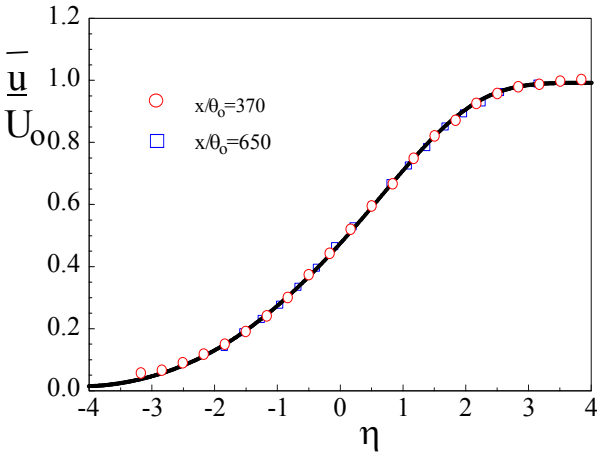

Figure 4. Mean velocity profile in the shear layer

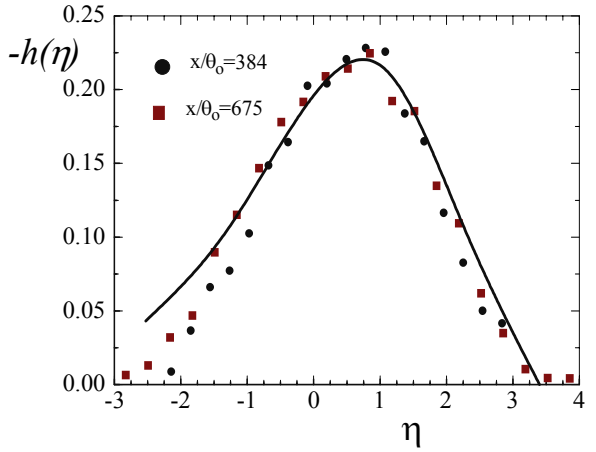

Figure 5. Calculated and measured Reynolds shear stress

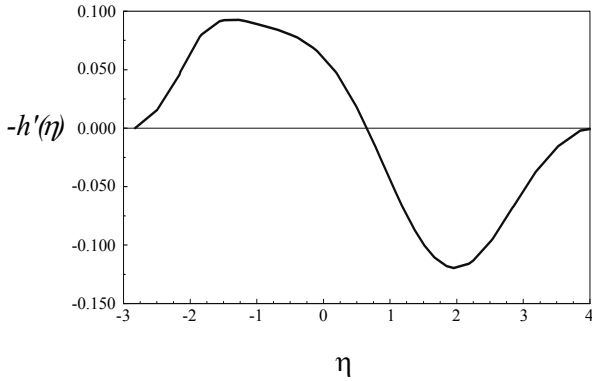

Figure 6. Reynolds stress gradient, obtained by fitting and differentiating the data shown in Fig. 5.

The wave number content of the present measurements will be used to characterize the physical attributes of this flow field. The first of these measures is the u-v coherence spectra, see Fig.4. As shown, a necessary condition for "local isotropy" is met for $k_1\eta>0.01$. The E_{11} power spectral density (PSD) is presented in Fig. 5 with the "best fit" reference curve, obtained using the procedure of Pope (2000), included for reference.

A more sensitive (pre-multiplied by k_1) representation of the component spectra $k_1E_{\gamma\gamma}(k_1\eta)$ is presented in Fig 6 for γ= 1, 2, 3. Note that when spectra are plotted in this form, equal areas "under the curve" contribute equally to the signal variance. As expected the E_{11} values exhibit the largest magnitudes at low wave number.

Fig. 7 presents a segment of the complete time record acquired for the $\omega_z(t)$ magnitudes at η=0.508. This quantity can be described using the Reynolds decomposition: $\omega_z(t) = \overline{\omega_z} + \omega'_z(t)$. Quite unlike the velocity distributions the $\tilde{\omega}_z/\overline{\omega_z}$ are quite large (≈22 at this location). It is instructive to consider not only the large fluctuation levels but also the rapidly changing values. It is implied that the instantaneous vorticity field is highly stretched by the velocity field $[\vec{V}\cdot\nabla\vec{\omega}]$.

Fig. 8 presents the pre-multiplied vorticity spectral distributions. Since the area under the curve in this representation is the normalized mean square vorticity value, the evident differences in the indicated area reflects the difference in the normalized standard deviations for ω_z and ω_y 0.92 cf 0.58, respectively. The other noteworthy features of Fig. 7 are:

i) quite similar magnitudes for $k_1\eta>0.2$,

ii)a peaked ω_y spectra (at $k_1\eta$=0.15) is evident whereas the ω_z spectra is "nominally invariant" over a wide range of k_1 values.

The velocity-vorticity co-spectral distributions that directly address the Reynolds stress gradients are shown in Fig. 9. The v, ω_z cospectra clearly shows larger values in the low k_1 ($k_1\eta$=0.001) region. These values are essentially responsible for the larger $\overline{v'\omega_z'}$ value (221 m/sec^2 or $\theta\overline{v'\omega_z'}/U_o^2$=0.199) that stands in contrast to the $\overline{w'\omega_y'}$ value (141 m/sec^2 or $\theta\overline{w'\omega_y'}/U_o^2$=0.087). The strong similarity of the pre-multiplied E_{22}, E_{33} spectra, in contrast with the different low frequency content of the vorticity-velocity spectra, clearly identify the mechanistic contributors to the Reynolds stress gradients. Namely, the motions whose $k_1\eta$ values are of order 10^{-3} primarily contribute to the Reynolds stress gradient.

The scaling used above: [θ and U_o], result in a non-dimensional difference for the rhs of Equation 3 as:

$$\frac{\theta}{U_o^2}[\overline{v'\omega_z'} - \overline{w'\omega_y'}] = 0.199 - 0.087 = 0.112\,.$$

This magnitude can be compared with the measured gradient:

$$\frac{\partial}{\partial(y/\theta)}\left[\frac{\overline{u'v'}}{U_o^2}\right] = 0.0021$$

The implication of these data is quite apparent. It will not be feasible to use the rhs of (3) to accurately predict the numerical value of the Reynolds stress gradient given the intrinsic uncertainties in the measurement, and the ill conditioned nature of equation (3). That is, the left hand side is several orders of magnitude smaller than the individual terms on the right hand

side. Therefore any uncertainty in the velocity-vorticity products will result in a difference that is far greater than the true stress gradient. However, the clearly stated identification of the wave number range that contributes to this quantity provides quite useful insight into the mechanistic attributes that lead to the observed mean velocity field.

SUMMARY

Detailed measurements of the vorticity velocity products have shown that motions whose scales are $\approx 10^{-3}\eta$ dominantly contribute to the Reynolds shear stress gradients at the center of this flow field. This range is one of order of magnitude smaller than the domain where local isotropy could be expected ($H_{12}\approx 0$ at $k_1\eta > 0.01$).

ACKNOWLEDGEMENTS

Financial support for the construction of the experimental facility was provided by the Ford Motor Co., Mr. F Manani. Partial salary support for the S.C. Morris Ph.D studies was obtained from Daimler Chrysler, Caterpillar, and the office of Naval Research (ONR subcontract through the University of Utah: No 2004092).

REFERENCES

Haw, R.C., Foss, J.K., Foss., J.F., 1989, "Vorticity based intermittency measurements in a single stream shear layer," in Advances in Turbulence 2, eds. Fernholz, H., and Fiedler, H., Springer-Verlag, Berlin.

Pope, S., 2000, Turbulent Flows, Cambridge University Pres.

Tennekis and Lumley, 1972, A First Course in Turbulence, MIT Press.

Wallace, J.M., Foss, J.F., 1995, "The Measurement of Vorticity in Turbulent Flows," *Annu. Rev. Fluid Mech*. 27, pp469-514.

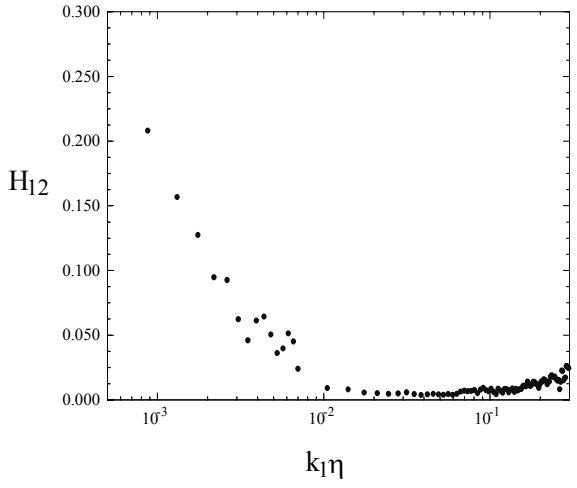

Figure 4. Coherence function: $E_{12}^2 / E_{11} E_{22}$

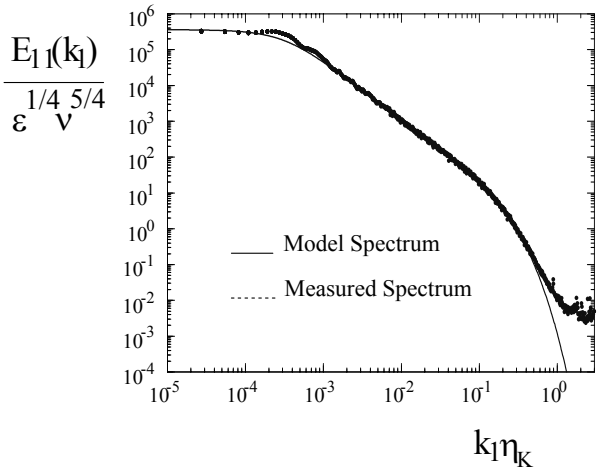

Figure 5. Power Spectral density E11 with model fit from Pope (2000).

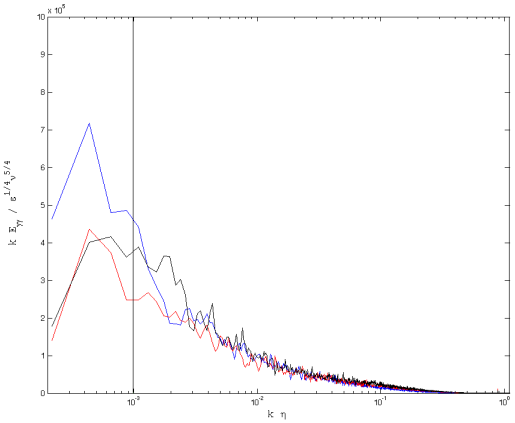

FIgure 6. Pre-multiplied power spectral densities for $\gamma\gamma$=11 (top curve at $k_1\eta=10^{-3}$), $\gamma\gamma$=22 for the middle curve at $k_1\eta=10^{-3}$, and $\gamma\gamma$=33 for the lower curve.

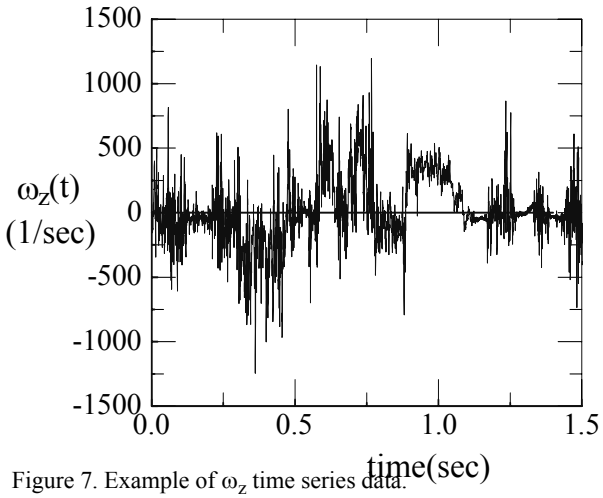

Figure 7. Example of ω_z time series data.

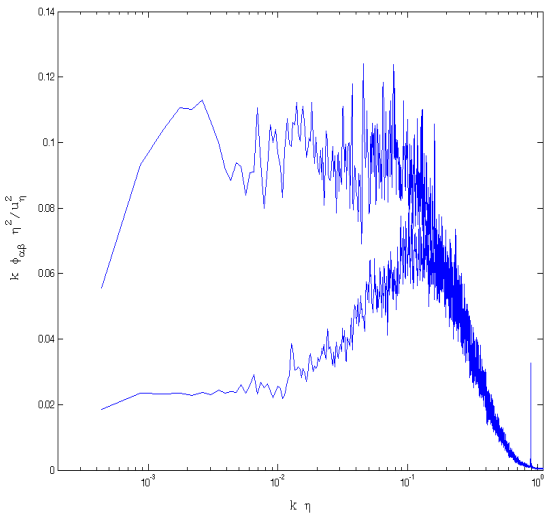

Figure 8. Pre-multiplied spectral distributions of the $\alpha=\beta=\omega_z$ (upper) and $\alpha=\beta=\omega_y$ (lower).

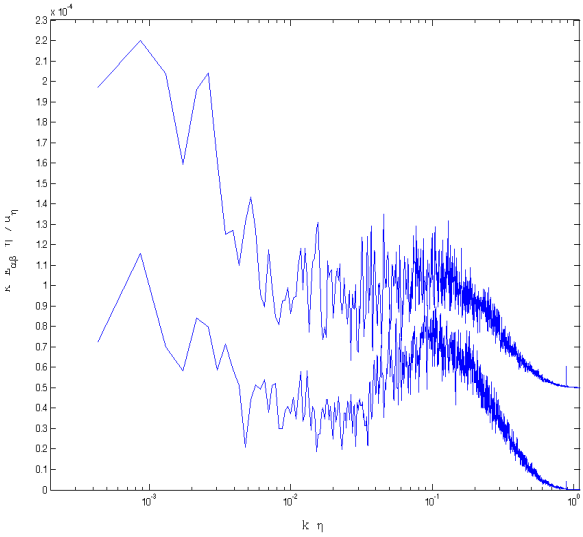

Figure 9. Velocity (α) - vorticity (β) spectra where the lower curve shows $\alpha=w$, $\beta=\omega_y$, and the upper curve shows $\alpha=v$, $\beta=\omega_z$. The values of the upper curve are shifted upward by 0.5 to separate the two distributions.